Nonlinear Modelling of an F16 Benchmark Measurement

Péter Zoltán Csurcsia[1], Jan Decuyper[1], Balázs Renczes[2], Tim De Troyer[1]

[1] Department of Engineering Technology (INDI)
Vrije Universiteit Brussel (VUB)
Pleinlaan 2, B-1050 Elsene, Belgium

[2] Department of Measurement and Information Systems (MIT)
Budapest University of Technology and Economics (BME)
Magyar tudósok krt. 2, H-1117 Budapest

ABSTRACT
Engineers and scientists want mathematical models of the observed system for understanding, design and control. Many mechanical and civil structures are nonlinear. This paper illustrates a combined nonparametric and parametric system identification framework for modeling a nonlinear vibrating structure. First step of the process is the analysis: measurements are (semi-automatically) preprocessed, and a nonparametric Best Linear Approximation (BLA) method is applied. The outcome of the BLA analysis results in nonparametric frequency response function, noise and nonlinear distortion estimates. Second, based on the information obtained from the BLA process, a linear parametric (state-space) model is built. Third, the parametric model is used to initialize a complex Polynomial Nonlinear State-Space (PNLSS) model. The nonlinear part of a PNLSS model is manifested as a combination of high-dimensional multivariate polynomials. The last step in the proposed approach is the decoupling: transforming multivariate polynomials into a simplified, alternative basis, thereby significantly reducing the number of parameters. In this work a novel filtered canonical polyadic decomposition (CPD) is used. The proposed methodology is illustrated on, but of course not limited to, a ground vibration testing measurement of an F16 aircraft.

Keywords: MIMO systems, nonlinearity, decoupling, system identification, ground vibration testing

1. INTRODUCTION

This paper illustrates a combined nonparametric and parametric system identification framework for modeling nonlinear vibrating structures. The proposed methodology is illustrated on – but not limited to – a ground vibration testing (GVT) measurement of an F16 aircraft. Many mechanical and civil structures are inherently nonlinear. The problem lies in the fact that there are many different types of nonlinear systems, each of them behaves differently, therefore modelling is very involved, and universally usable design and modelling tools are not available. For these reasons the nonlinear systems are often approximated with linear systems, because its theory is user friendly and well understood. For an overview of the nonlinear modeling techniques we refer to [1, 2] and [3].

The first step is the data analysis: measurements are (semi-automatically) preprocessed, and a nonparametric Best Linear Approximation (BLA) method is performed. The nonparametric Best Linear Approximation (BLA) framework will be used as a first step [4]. The outcome of the BLA analysis results in a nonparametric frequency response function together with noise and nonlinear distortion estimates.

The considered nonlinear model is a polynomial nonlinear state-space (PNLSS) model which consists of the classical linear state-space part (initialized by BLA FRF) and a nonlinear extension. The PNLSS model structure is flexible, as it can capture many different nonlinear dynamic behaviors. However, it suffers from the issue that even for a moderate complexity problem, there are an excessive number of parameters needed.

To overcome this issue, a filtered canonical polyadic decomposition-based decoupling is applied: transforming multivariate polynomials into a simplified representation, thereby reducing the number of parameters.

In this work multisines are considered as excitation signals. The advantage of the multisines is that 1) there is no problem with spectral leakage/transient, 2) they result in high quality frequency response functions (FRFs), and 3) they provide easy-to-understand information about the nonlinearities.

The numeric results of the nonparametric (and partly the parametric) work are obtained by the use of the SAMI (Simplified Analysis for Multiple Input Systems) toolbox [5]. The initial PNLSS models are obtained by the freely available PNLSS toolbox [6]. In this work, however, we focus on high level understanding, instead of the usage of the toolbox or elaborating formulas.

This paper is organized as follows. Section 2 briefly describes the considered systems and the main assumptions applied in this work. Section 3 discusses the nonparametric BLA estimation framework. The parametric polynomial nonlinear state-space model is elaborated in Section 4. In Section 5 the description and analysis of the GVT experiments of an aircraft are given. Conclusions can be found in Section 6.

2. BASICS

The dynamics of a linear multiple-input, multiple output (MIMO) system can be nonparametrically characterized in the frequency domain by its Frequency Response Matrix (FRM) [7] G at discrete frequency index k, which relates the inputs U to outputs Y as follows:

$$Y(k) = G(k)U(k) \tag{1}$$

In this work are BIBO (bounded-input, bounded-output) stable physical systems [8]. For the sake of simplicity, the frequency indices will be omitted, and it is assumed to understand each quantity at frequency index k.

This system represented by G is linear when the superposition principle is satisfied in steady-state, i.e.:

$$Y = G(a+b)U = GaU + GbU = (a+b)\,GU \tag{2}$$

where a and b are scalar values. If G does not vary, for any a, b (and excitation), then the system is called linear-time invariant (LTI). On the other hand, when G varies with a and b (and the variation depends also on the excitation signal – e.g. level of excitation, distribution, etc.) then the system is called nonlinear.

Because time-varying systems are often misinterpreted as nonlinear systems, it is important to mention that when G varies over the measurement time, but at each time instant the principle of superposition is satisfied, then the system is called linear time-varying (LTV) [9] [10] [11].

In this work we consider nonlinear time-invariant stable (damped) mechanical (vibrating) systems, and the output of the underlying system has the same period as the excitation signal (i.e. the system has PISPO behaviour: period in, same period out [12]).

Further, it is assumed that the excitation signal is known (measured precisely), the actuator of the system is linear.

3. DESIGN OF EXPERIMENT

Multisine excitation and detection of nonlinearities

In modern system identification, special excitation signals are available to assess the underlying systems in a user-friendly, time efficient way [13]. To avoid any spectrum leakage, to reach full nonparametric characterization of the noise, and to be able to detect nonlinearities, a periodic signal is needed. The best signal that satisfies the desired properties is the user-friendly multisine signal (see Figure 1) which looks like Gaussian white noise, behaves like it but it is not noise. The random phase

(uniformly distributed) multisine is a sum of harmonically related sinusoids. The amplitude distribution of a random phase multisine is approximately normal (it approaches a Gaussian distribution as the number of harmonics tend to infinity). Note that this signal is also known as pseudo-random (multisine) signal [12].

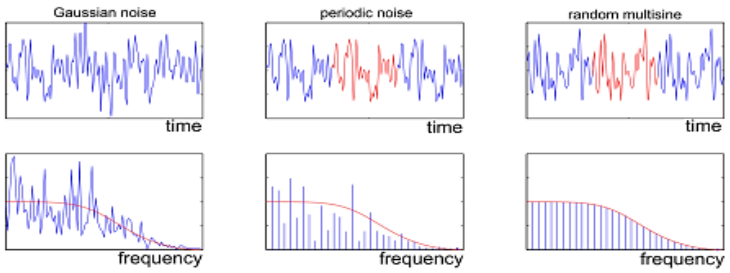

Figure 1: Different excitation signals in time and in frequency domain

4. BEST LINEAR APPROXIMATION

Theoretical structure and the basic assumptions

The Best Linear Approximation (BLA) has been widely used in the last decades to efficiently estimate FRFs [13]. The BLA of a nonlinear system is an approach of modelling that minimizes the mean square error between the true output of a nonlinear system and the output of the linear model.

The proposed BLA technique makes use of the knowledge that the excitation signal has both stochastic and deterministic properties. In this work the excitation signal is a random phase multisine signal and it is assumed to be measured precisely. In each measurement there are *m* different random realizations of multisines and each of the realizations is repeated *p* times. The BLA estimate consists of several components. Figure 2 shows the theoretical structure of the considered BLA estimator.

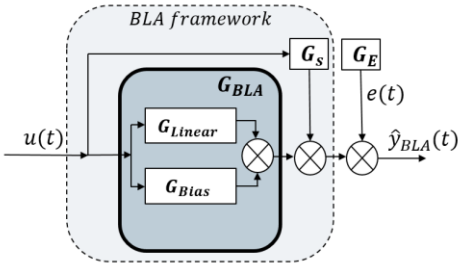

Figure 2: The theoretical structure of the best linear approximation

G_{Linear} is the linear (transfer function) component of BLA. This component is phase coherent: harmonic-wise random phase rotation in the input excitation would result in a proportional phase rotation at the output.

In case of non-coherent behaviour, the input phase rotation would result in a random phase rotation at the output. Please note that significant part of the nonlinearities is non-coherent. When many input phase rotations are performed, the random output rotations can be seen as an additional (nonlinear) noise source (G_S) next to the ordinary measurement noise (G_E) – assumed to be additive i.i.d. normal distributed with zero mean with a finite variance. The unmodelled nonlinearities results in a bias term (G_{bias}). The usage of periodic excitation reduces the effects of the measurement noise G_E. The usage of multiple random phase realizations reduces the level of non-coherent nonlinearities.

Two-dimensional averaging

When the BLA estimation framework is applied, the observed system is excited by random phase multisines. In this work there are *m* different realizations of the multisine excitation signal, each realization is repeated *p* period times. The considered steady-state model in frequency domain at frequency bin index *k* is given by:

$$\hat{G}^{[m][p]} = \hat{Y}^{[m][p]}_{measured} \mathrm{U}^{[m]^{-1}} = \hat{G}_{BLA} + \hat{G}_S^{[m]} + \hat{G}_E^{[m][p]} \quad (3)$$

The steady state signals are obtained in this work by discarding some periods at the beginning of each realization block. In order to estimate the underlying system one has to average over *p* periods of repeated excitation signal, and over the *m* different realizations of the excitation signal [12] (see Figure 3).

First, let us average over the *p* periods of a realization. If *p* is sufficiently large then (considering the law of large numbers and the distribution properties of the observation noise) the expected value of $\hat{G}_E^{[m][p]}$ converges to zero, so that this term is eliminated. In other words, averaging over repeated blocks results in an improvement of the SNR. Because the stochastic nonlinear contributions $\hat{G}_S^{[m]}$ does not vary over the repetition of the same realization we have to average over the *m* different realizations. If *m* is sufficiently large, then $\hat{G}_S^{[m]}$'half-stochastic' nonlinear noise source converges to zero, so that term is eliminated. After the 2D averaging the BLA estimate is obtained.

The estimate of the noise sample variance $\hat{\sigma}^2_{G_E}$ is calculated from the averaged sample variance of each realization. The total variance of the FRM $\hat{\sigma}^2_{\hat{G}_{BLA}}$ is calculated from the sample variance of each different partial BLA estimates $\hat{G}^{[m]}$.

The difference between the total variance and the noise variance is an estimate of the variance of the stochastic nonlinear contributions $\hat{\sigma}^2_{NL} \approx (\hat{\sigma}^2_{\hat{G}_{BLA}} - \hat{\sigma}^2_{G_E})$.

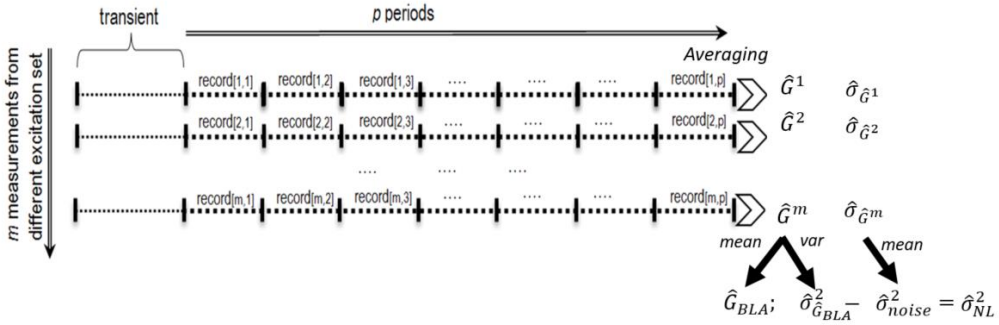

Figure 3: Evaluation of BLA estimate with the help of 2D averaging

Using the proposed 2D averaging technique the influence of the noise and nonlinear contribution can be decreased, and the final result is the BLA FRF estimate. In [7] it has been suggested to choose the number of periods more than one ($p \geq 2$) and the different realizations more than six ($m \geq 7$). Detailed calculations of the proposed 2D approach can be found in [14].

5. POLYNOMIAL NONLINEAR STATE-SPACE MODEL

A polynomial nonlinear state-space (PNLSS) model consists of the classical linear state-space part and the nonlinear extension part where auto and cross terms of the input and states are considered, see Figure 4.

It is based on the work of [15, 16]. It estimates and simulates polynomial PNLSS models from measured data. The PNLSS model structure is flexible, as it can capture many different nonlinear dynamic behaviors (hysteresis, nonlinear feedback, etc.).

The model structure can also easily deal with multiple inputs. The method has already been successfully applied in a large range of applications (mechanical, electronical, electrochemical). Because of the state-space representation it is suitable for control and simulation. The main concern is that the PNLSS is extremely sensitive to unseen input distribution and it might produce unstable simulation output. The foundation of these issues can be seen when looking at the lower level: the kernel of these models is a high-dimensional multivariate polynomial nonlinear function.

A possible solution to this problem is discussed next.

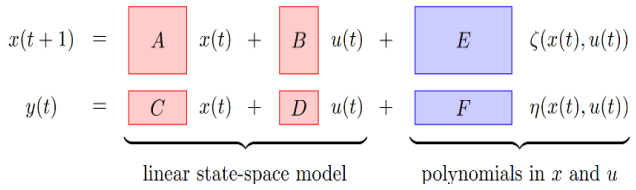

Figure 4: The theoretical structure of PNLSS model.

6. DECOUPLING

Decoupling aims at transforming generic multivariate nonlinear functions into decoupled functions. The decoupled structure is characterized by the fact that the relationship is described by a number of univariate functions of intermediate variables. Decoupling is designed to post-process multivariate nonlinearities which emerge naturally in a large number of dynamical models. The objective is to achieve model reduction while gaining insight into the nonlinear mapping [17]. Given a generic nonlinear function

$$q = f(p) \tag{4}$$

with $q \in \mathbb{R}^n$ and $p \in \mathbb{R}^m$, the idea is to introduce an appropriate linear transformation of p, denoted V, such that in this alternative basis, univariate functions may be used to describe the nonlinear mapping. The rationale behind the method is that classical regression tools, e.g. a polynomial basis expansion, not necessarily result in a sparse representation. By allowing a rotation towards a more favorable basis, a more efficient representation can be obtained. The decoupled function is then of the following form

$$f(p) = Wg(V^T p) \tag{5}$$

where the *i*th function is $g_i(z_i)$ with $z_i = v_i^T p$, emphasising that all functions are strictly univariate. The number of univariate functions, denoted r, is a user choice which can be used to control the model complexity (r may be larger or smaller than n). It plays a crucial role since it will determine whether the implied equivalence of (5) can be attained. A second linear transformation W maps the function back onto the outputs. The matrices then have the following dimensions: $V \in \mathbb{R}^{m\,x\,r}$ and $W \in \mathbb{R}^{n\,x\,r}$. The decoupled structure is represented graphically in Fig 5.

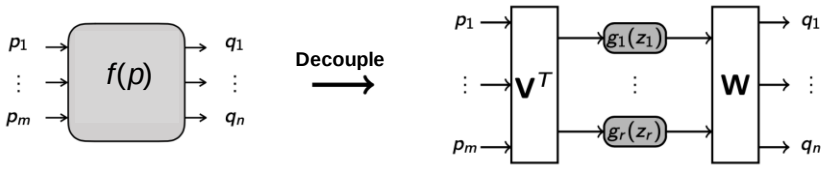

Figure 5: Illustration of the decoupling technique.

Decoupled functions have a number of attractive features. The fact that the nonlinearity is captured by a set of univariate functions enables to easily visualize the relationship. This may lead to insight. Moreover, decoupled functions are often a much more efficient parameterization of the nonlinearity, resulting in a significant reduction in the number of parameters.

In this work, the filtered CPD approach of [18] is used to decouple the multivariate polynomial present in the state equation, $E\zeta(x,u)$ in Fig. 3. The algorithm links the original function to a decoupled function on the basis of its first order derivative information. The method relies on the underlying diagonal structure of the Jacobian, which is a consequence of using univariate functions g_i. Applying the chain rule, one obtains the Jacobian of (5)

$$J' = W\text{diag}([h_1(z_1) \ \ldots \ h_r(z_r)])V^T \tag{6}$$

[19] found that the underlying diagonality of the Jacobian can be exploited in the decoupling process. It was suggested to construct a third order tensor, $\boldsymbol{\mathcal{J}}$, out of evaluations of the Jacobian of the known function, $\boldsymbol{f}(\boldsymbol{p})$, and compute a diagonal decomposition, denoted $\boldsymbol{\mathcal{J}}'$, such that $\boldsymbol{\mathcal{J}} \approx \boldsymbol{\mathcal{J}}'$. The tensor decomposition is depicted in Figure 6.

The decomposition returns three matrix factors: both the required linear transformation matrices *W* and *V*, together with a third matrix *H* which stores nonparametric estimates of the first order derivative of the functions g_i.

In [18], the decomposition was modified by introducing finite difference filters. This allows for the Jacobian tensor to be decomposed into the more convenient factors $\{W, V, H'\}$, where H' directly stores evaluations of the univariate functions g_i. The method of [18] can be summarized in three steps:

1. Evaluate the Jacobian of the known function, J, in a number of operating points and stack the matrices into a three-way array, i.e. the Jacobian tensor $\mathcal{J} \in \mathbb{R}^{n \times m \times N}$.
2. Factor $\mathcal{J}$ into $\{W, V, H'\}$ by computing a filtered diagonal tensor decomposition (F-CPD).
3. Retrieve the functions, g_i, by parametrizing the nonparametric estimates stored in H'.

The filtered CPD approach is a generic tool which can be used to retrieve decoupled functions, regardless of the function family. Irrespective of the size of the function in terms of *m* and *n*, the decoupling procedure boils down to solving a third order tensor decomposition. Only in a final parameterization step, an appropriate basis function is selected for the univariate branches. An additional advantage of the filtered CPD is that the method no longer relies on the uniqueness properties of tensor decomposition. The result is that meaningful decompositions, pointing towards decoupled functions, can be obtained for a user chosen value of *r*, enabling to control the model complexity.

The results illustrate that the nonlinear functions found in PNLSS models may typically be replaced by decoupled functions with a low number of univariate branches. This alludes to the fact that nonlinear dynamical systems are in many cases driven by a low number of internal nonlinearties.

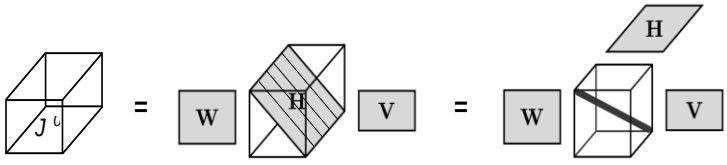

Figure 6: Illustration of the decoupling technique. Center: a collection of evaluations of the Jacobian of the decoupled function, stacked in the third dimension. Left: corresponding third order tensor. Right: extracting the diagonal plane reveals a diagonal tensor decomposition.

7. EXPERIMENTAL ILLUSTRATION

F16 measurement

This section concerns the ground vibration testing measurement campaign of a decommissioned F-16 aircraft with two dummy payloads mounted at the wing tips, see Figure 8. The detailed description of the measurement and benchmark data are openly accessible [20].

The right wing is excited by a shaker using combined multisines: odd multisines with skipping one random bin within each group of 4 successively excited odd lines. This sparse grid is used to detect even and odd nonlinear contributions. The sampling frequency is 400 Hz, the period length 16384 samples. The reference (voltage), input (force) and output (acceleration) signals are measured. The range of excitation is between 1 and 60 Hz, there are 3 periods and 9 realizations per excitation level. There are 3 different input levels measured at 12.2, 49.0 and 97.1 N RMS.

In the 1 – 15 Hz band, the aircraft possesses about 10 resonance modes. The first few modes below 5 Hz correspond to rigid body motions of the structure. The first flexible mode around 5.2 Hz corresponds to wing bending deformations. The mode involving the most substantial nonlinear distortions is the wing torsion mode located around 7.3 Hz: the mounting interface of

the payload features nonlinearities in stiffness and damping, due to clearance and friction. Therefore, the models are estimated for the frequency range of interest (4.5…15 Hz) at the payload connection.

Figure 7: F-16 ground vibration testing measurement campaign. The right wing is excited by a shaker. Major part of the nonlinearities is related to the payload connection.

Data processing

The data processing is fully automated by the toolbox: segmentation of data, trends (such as the mean/offset values) from the individual segments are removed [13], the transient is analyzed.

Figure 8 shows the visualization of toolbox transient check-up routine. The left side of the figure shows the acceleration (output) measurement at the payload connection. In order to determine the length of the transient (i.e. the number of delay blocks), the last block (period) – assumed to be nearly in steady-state – is subtracted from every preceding block. Because the transient decays as an exponential function, the differences are shown in logarithmic scale [13].

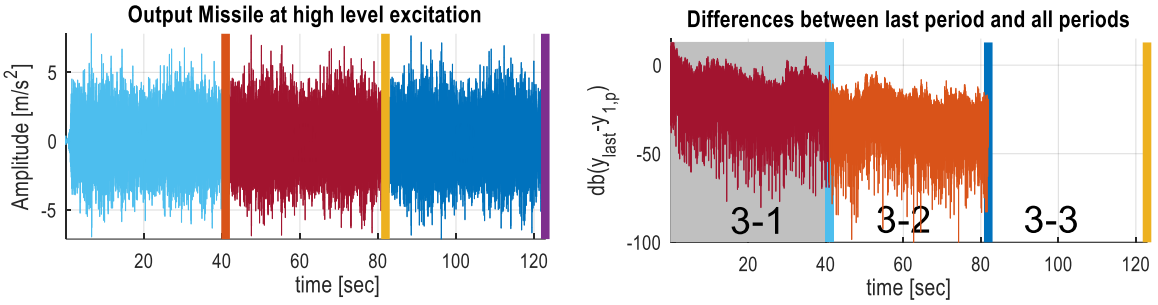

Figure 8: Periodicity at the payload connection. The left figure shows the block repetitions (accelerometer data). The right figure shows the differences between the last block minus every block in dB scale. Observe in the second figure the fast decay in the first few seconds (this is the transient). The greyed area refers to the automatically detected transient (delay) block which will be discarded during the processing of the measurement. Please note that the automated transient check involves all available signals.

Reference and Input signals

The reference and input signals are shown in Figure 9, the low, medium and high level of excitation. The left figure shows the generated reference (voltage) signals and their noise estimates. This measurement has very good quality (SNR is greater than 75 dB), the even and odd nonlinear distortions are hidden in the noise.

The excitation forces (see right figure) are measured with approximately 50…80 dB SNR. It is interesting to point out that the highest input signal is 18 dB higher than the lowest one, but the SNR is decreased with around 8 dB. This indicates the presence of (weak) nonlinearities at the excitation system.

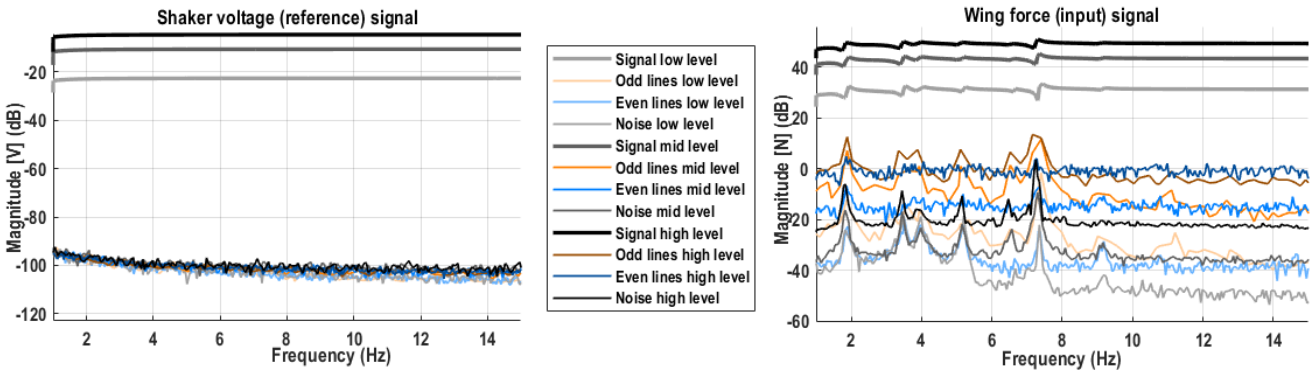

Figure 9: The measured reference (voltage), input (force) signals are shown. Darker shades refer to higher excitation levels. Thick grey shades refer to the signals. Thin grey shades refer to noise estimates. Orange shades (on signal measurements) refer to the odd distortions. Blue shades (on signal measurement) refer to the even distortions.

Payload measurement

Further, in order to simplify the analysis, the output and FRF are shown at the payload connection only. The output (acceleration) measurements are shown in Figure 10. As can be seen, the SNR is around 40…50 dB at the resonances. At the higher excitation level, the SNR decreased with approximately 10 dB w.r.t the lowest level excitation.

It can also be observed that the resonances have been shifted, which is also a further indication of nonlinearities. This is due to the fact, that at higher level of excitation we have dominant odd distortions, which usually manifest in changing resonance locations and shapes (it is the so-called hardening or softening stiffness nonlinear effect). Please note that even distortions usually manifest as excessive noise on the measurement.

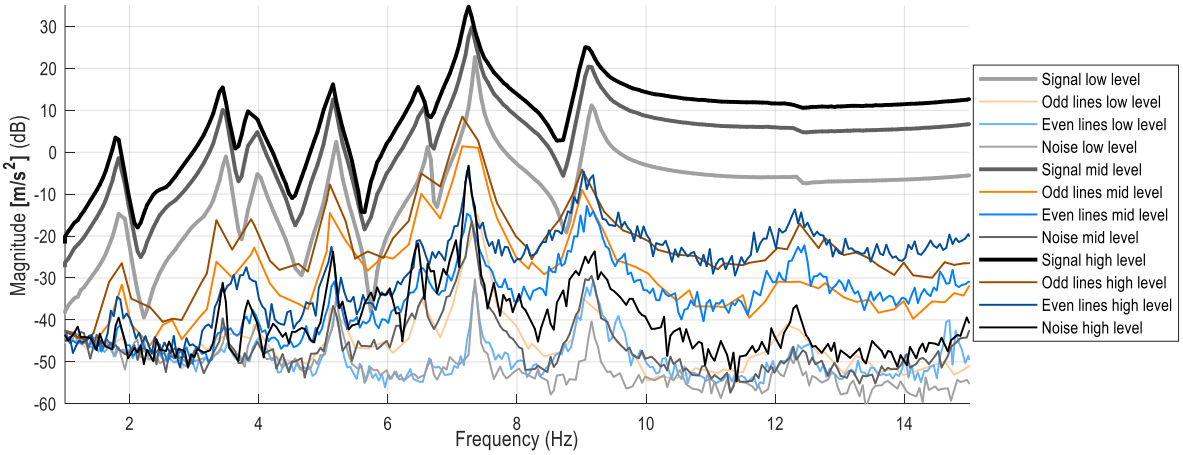

Figure 10: The output (acceleration) measurement shown at the payload connection. Darker shades refer to higher excitation levels. Thick grey shades refer to the signals. Thin grey shades refer to noise estimates. Orange shades (on signal measurements) refer to the odd distortions. Blue shades (on signal measurement) refer to the even distortions. Observe that the higher the excitation, the more the dominance of odd nonlinear distortions.

FRF analysis

Figure 11 shows the FRFs at low and high level of excitation. This is the classical approach, FRFs at multiple levels of excitation are compared with each other. It is interesting to point out that despite the fact that the high excitation is only 18 dB higher than the lowest level excitation, it can be clearly observed that FRFs at different levels differ a lot from each other, for instance shifting resonances and varying damping. This clearly indicates the presence of nonlinearities. The usage of the proposed multisines allows us to obtain noise and nonlinearity level estimations as explained earlier. For instance, when looking at the high level excitation case, the most dominant resonance (around 7.3 Hz) has an approximate SNR of 43 dB, and an SNLR (signal-to-nonlinearity ratio) of 15 dB. This means that at that resonance the main error source is the nonlinearity.

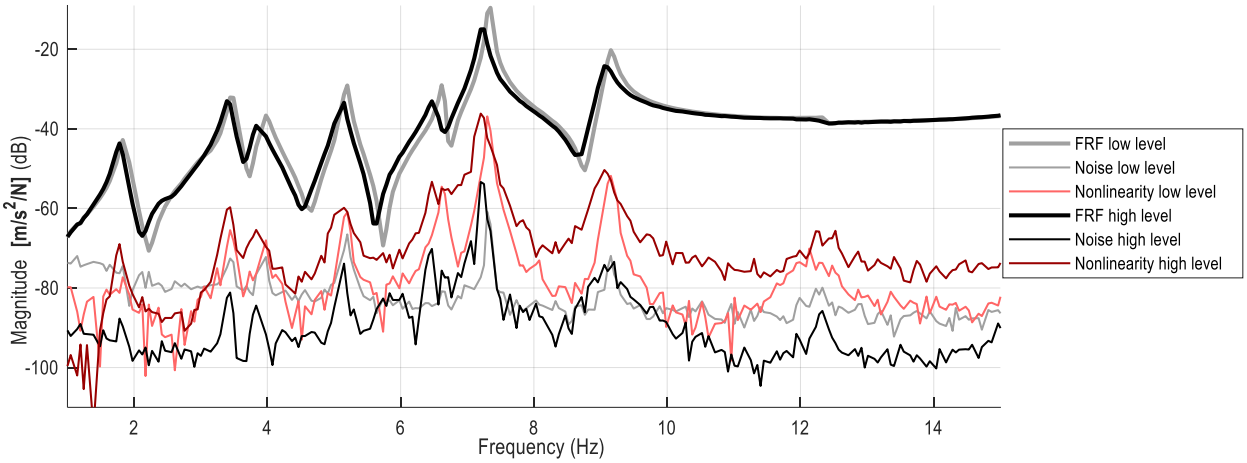

Figure 11: The FRF estimation shown at the payload-right wing connection. Darker shades refer to higher excitation levels. Thick grey shades refer to the FRFs. Thin grey shades refer to noise estimates. Red shades refer to the nonlinear distortions.

Post-processing

The next step is the parametric post-processing of the data. In order to reduce the computational needs 9 realizations were taken from low and high level. In each realization the periods were averaged (and the resulting data are split into):

- estimation dataset: 4-4 realizations (to build a model),
- validation dataset: 4-4 realizations (to validate a model),
- test dataset: 1-1 realization (to compare different approaches).

Parametric BLA

A parametric (state-space) model is built based on low level nonparametric BLA (FRFs and noise) estimates. In order to determine the parametric model order (i.e. number of states), a cross-validated model order scanning method is used between orders 1 and 15 in the frequency range of interest. The best fit (see Figure 12.) w.r.t. cross-validation error was found with a model order of 12, resulting in a total of 169 parameters to be estimated (see Table 1).

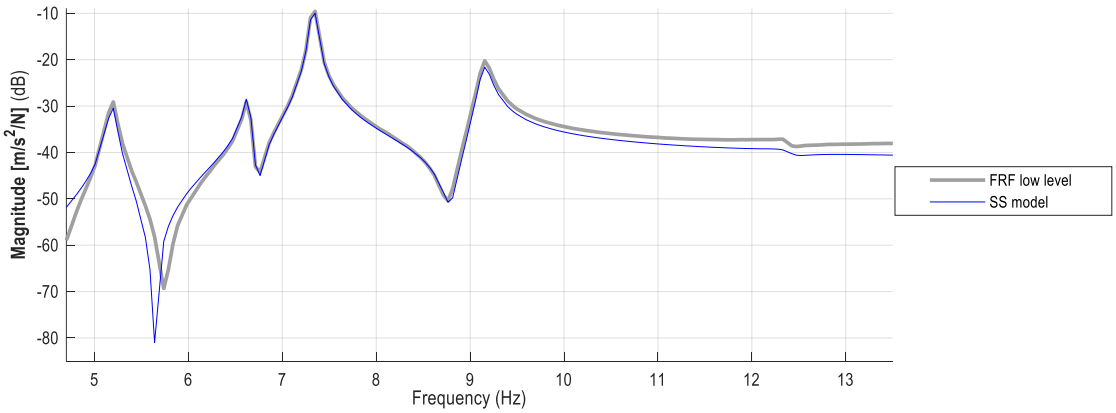

Figure 12: Parametric and nonparametric FRFs at driving point estimated at the low excitation level.

PNLSS model and decoupling

A PNLSS model is initialized with the help of the previously obtained parametric low level BLA model. In order to reduce the complexity of the problem and the computational needs, only matrix E (state nonlinearities) is considered with 2nd and 3rd order multivariate cross terms resulting in more than 6000 parameters. The PNLSS model is obtained using an optimization routine with 40 iteration steps [15] trained on the 4-4 low and high level realizations of the estimation dataset. Applying the F-CPD method to the function of the nonlinear part of the PNLSS model $E\zeta(x,u)$ reduces the number of nonlinear parameters

from 6552 to 29. Decoupling method has been applied to obtain one univariate branch based on the full PNLSS model. The resulting reduced order model was post-optimized.

Discussion of results

The performance of the parametric, nonparametric BLA and PNLSS and decoupled models are detailed in Table 1. A model fitting on a high level data segment is shown in Fig 13. Observe that the worst results are obtained with the nonparametric BLA FRF model: the relative rms error is always above 100% (at high level above 200%). The nonparametric model involved more than 400 parameters (FRF data points). The reduced order BLA SS model with 169 parameters provides already acceptable fit for low level of excitation (around 16% error), whereas at high level of excitation the error level is still above 100%. This is expected since the linear models were estimated only at the low excitation level. The PNLSS model provides already a good fit (with maximum error of 40%) at the cost of increased number of parameters (more than six thousand parameters). The best results are obtained with the decoupling technique, with less than 200 parameters, the relative error is maximum 8.8%.

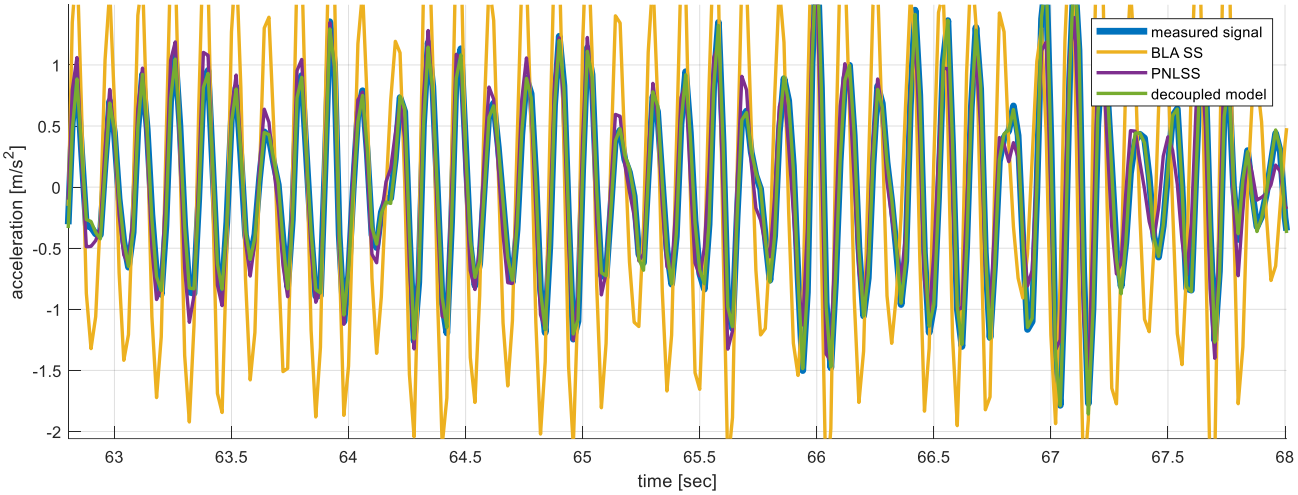

Figure 13: Fitting illustration on a segment of the test data.

Table 1. Overview of the results

Model	Relative rms error on test data		Number of parameters
	low level	high level	
Nonparametric BLA trained on low level	1.001	2.335	427
Parametric BLA trained on low level	0.162	1.132	169
Full PNLSS	0.082	0.400	169+6552
PNLSS with 2 branches - optimized	0.070	0.088	169+29

8. CONCLUSIONS

In this work a novel, semi-automated semi-parametric approach was developed to provide a user-friendly modeling tool for nonlinear benchmark data. The results turned out to be useful for modelling the nonlinear ground vibration testing of the aircraft because:

- it required minimal user-interaction, and no expert-user was needed
- the input, output and transfer function measurements were nonparametrically characterized
- high-dimensional PNLSS models were successfully decoupled resulting in a very compact powerful model.

ACKNOWLEDGEMENTS

This work was funded by the Strategic Research Program SRP60 of the Vrije Universiteit Brussel, and by the Flemish fund for scientific research FWO under license number G0068.18N.

REFERENCES

[1] G. Kerschen, K. Worden, A. Vakakis and J.-C. Golinval, "Past, present and future of nonlinear system identification in structural dynamics,," *Mechanical Systems and Signal Processing*, vol. 20, no. 3, pp. 505-592, 2006.

[2] K. Worden and G. Tomlinson, Nonlinearity in Structural Dynamics: Detection, Identification and Modelling,, Bristol: Institute of Physics Publishing, 2001.

[3] J. Schoukens and L. Ljung, "Nonlinear System Identification: A User-Oriented Road Map," *IEEE Control Systems Magazine*, vol. 39, no. 6, pp. 28-99, 2019.

[4] P. Z. Csurcsia, B. Peeters and J. Schoukens, "User-friendly nonlinear nonparametric estimation framework for vibro-acoustic industrial measurements with multiple inputs," *Mechanical Systems and Signal Processing*, vol. 145, 2020.

[5] P. Z. Csurcsia, B. Peeters, J. Schoukens and T. D. Troyer, "Simplified Analysis for Multiple Input Systems: A Toolbox Study Illustrated on F-16 Measurements," *Vibration*, vol. 3, no. 2, pp. 70-84, 2020.

[6] J. Schoukens, "Prof. Dr. Johan Schoukens website," Vrije Universiteit Brussels, 2018. [Online]. Available: http://homepages.vub.ac.be/~jschouk/. [Accessed 2020 1 1].

[7] R. Pintelon, J. Schoukens, System Identification: A Frequency Domain Approach, 2nd ed., New Jersey: Wiley-IEEE Press, ISBN: 978-0470640371, 2012.

[8] L. Ljung, System identification: Theory for the User, 2nd ed., New Jersey: Prentice-Hall, ISBN: 9780136566953, 1999.

[9] P. Z. Csurcsia and J. Lataire, "Nonparametric Estimation of Time-variant Systems Using 2D Regularization," *IEEE Transactions on Instrumentation & Measurement*, vol. 65, no. 5, pp. 1259-1270, 2016.

[10] P. Z. Csurcsia, J. Schoukens, I. Kollár, "Identification of time-varying systems using a two-dimensional B-spline algorithm," in *2012 IEEE International Instrumentation and Measurement Technology Conference*, Graz, Austria, 2012.

[11] P. Z. Csurcsia, J. Schoukens, I. Kollár, "A first study of using B-splines in nonparametric system identification," in *IEEE 8th International Symposium on Intelligent Signal Processing*, Funchal, Portugal, 2013.

[12] P. Z. Csurcsia, "Static nonlinearity handling using best linear approximation: An introduction," *Pollack Periodica* , vol. 8, no. 1, 2013.

[13] J. Schoukens, R. Pintelon, Y. Rolain, Mastering System Identification in 100 exercises, New Jersey: John Wiley & Sons, ISBN: 978047093698, 2012.

[14] M. Alvarez Blanco, P. Z. Csurcsia, K. Janssens, B. Peeters and W. Desmet, "Nonlinearity assessment of mimo electroacoustic systems on direct field environmental acoustic testing," in *International Conference on Noise and Vibration Engineering*, Leuven, 2018.

[15] J. Paduart, Identification of nonlinear systems using Polynomial Nonlinear State Space models, Belgium: PhD thesis, 2008.

[16] J. Decuyper, Nonlinear state-space modelling of the kinematics of an oscillating circular cylinder in a fluid flow, Belgium: PhD thesis, 2017.

[17] J. Decuyper, K. Tiels and M. R. a. J. Schoukens, "Retrieving highly structured models starting from black-box nonlinear state-space models using polynomial decoupling," *Mechanical Systems and Signal Processing*, vol. 146, 2021.

[18] J. Decuyper, K. Tiels, S. Weiland and J. Schoukens, "Decoupling multivariate functions using a non-parametric (Filtered-CPD) approach," Padova, Italy, 2021.

[19] P. Dreesen, M. Ishteva and J. Schoukens, "Decoupling multivariate polynomials using first-order information," *{SIAM} Journal on Matrix Analysis and Applications*, vol. 36, no. 2, pp. 864-879, 2015.

[20] J.P. Noël and M. Schoukens, "F-16 aircraft benchmark based on ground vibration test data," in *2017 Workshop on Nonlinear System Identification Benchmarks*, Brussels, Belgium, 2017.